Reaction Chemistry & Engineering

ROYAL SOCIETY OF CHEMISTRY

PAPER

View Article Online
View Journal | View Issue

Check for updates

Cite this: *React. Chem. Eng.*, 2023, **8**, 1449

Effects of the mixer shape in a flow-type supercritical hydrothermal reactor as evaluated by neutron radiography and CeO_2 nanoparticle synthesis

Kosei Sato,[a] Ryosuke Sasaki,[a] Bo Xie,[a] Seiichi Takami,*[a] Masaki Kubo,[b] Takao Tsukada,†[b] Katsumi Sugimoto,[c] Naoya Odaira,[d] Daisuke Ito[d] and Yasushi Saito[d]

Received 8th January 2023,
Accepted 27th March 2023

DOI: 10.1039/d3re00018d

rsc.li/reaction-engineering

The mixer shape in flow-type reactors plays a vital role when the reaction rate is much faster than the mixing rate. In this study, we performed neutron radiography measurements on a flow-type supercritical hydrothermal reactor to examine the water density profile of the mixer and to determine the mixing behavior of the supercritical water and reactant solution streams. We examined the mixing behavior of the conventional and proposed mixers under various flow conditions. We also performed supercritical hydrothermal CeO_2 nanoparticle synthesis under the same mixing conditions and evaluated the effects of mixing behavior on the sizes of the produced CeO_2 nanoparticles.

Introduction

Nanoparticle synthesis has attracted considerable attention over the past few decades because nanomaterials exhibit different physical and chemical properties than their corresponding bulk materials and thus are expected to have many applications.[1–3] In particular, metal oxide nanoparticles are expected to be used in catalysts, batteries, medicine, sensors, and composite materials.[4,5] To date, various approaches for metal oxide nanoparticle synthesis have been proposed, such as sol–gel, spray pyrolysis, hydrothermal, solvothermal, and solid-state reactions. Among these approaches, hydrothermal synthesis is a unique method for producing metal oxide nanoparticles by heating an aqueous solution of metal ions to 100 °C or higher in a batch-type high-pressure reactor.[6,7] During hydrothermal synthesis, metal ions react with water at elevated temperatures to initially produce metal hydroxides that are successively dehydrated to produce metal oxide nanoparticles (Fig. 1a). Supercritical hydrothermal synthesis,[8–12] through which metal oxide nanoparticles are synthesized at temperatures higher than the critical temperature of water (374 °C), has also attracted much attention because the higher reaction rate and lower relative permittivity of water[13] (Fig. 1b) under these synthetic conditions result in a higher concentration and lower solubility of the products. As a result, a higher degree of supersaturation is realized, which leads to the synthesis of smaller nanoparticles with a narrower size distribution.

Supercritical hydrothermal metal oxide nanoparticle synthesis has been performed using either batch-type or flow-type reactors.[4,14,15] In flow-type reactors (Fig. 2a), a stream of water is supplied using a high-pressure pump and heated to several hundred degrees (°C) in a furnace. Simultaneously, a stream of aqueous metal ion solution is supplied using another high-pressure pump. The two streams are mixed in a mixer to instantaneously heat the aqueous metal ion solution

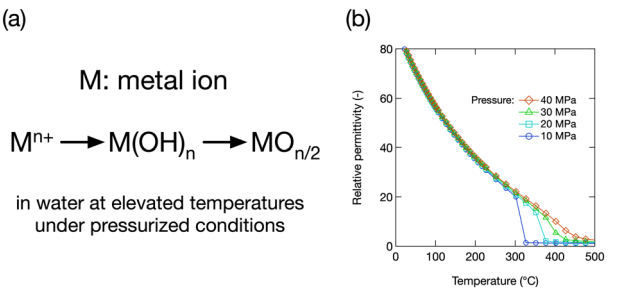

Fig. 1 (a) Scheme of hydrothermal synthesis and (b) the relative permittivity of water.[13]

[a] *Graduate School of Engineering, Nagoya University, Furo-cho, Chikusa-ku, Nagoya 464-8603, Japan. E-mail: takami.seiichi@material.nagoya-u.ac.jp*
[b] *Graduate School of Engineering, Tohoku University, 6-6-07, Aramaki Aza Aoba, Aoba-ku, Sendai 980-8579, Japan*
[c] *Graduate School of Engineering, Kobe University, 1-1 Rokkodai, Nada, Kobe 657-8501, Japan*
[d] *Institute for Integrated Radiation and Nuclear Science, Kyoto University, 2-1010, Asashiro-Nishi, Kumatori-cho, Sennan-gun, Osaka 590-0494, Japan*
† Current affiliation: New Industry Creation Hatchery Center, Tohoku University, 6-6-10, Aramaki Aza Aoba, Aoba-ku, Sendai 980-8579, Japan.

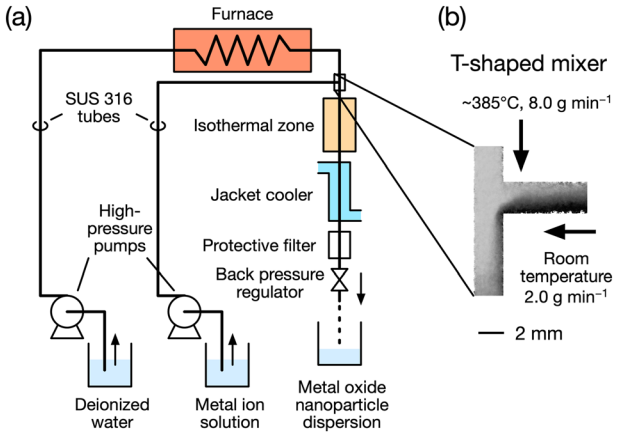

Fig. 2 (a) Schematic of a flow-type hydrothermal reactor and (b) the density profile of water in a conventional T-shaped mixer reported previously.[21]

to the reaction temperature. After passing through an isothermal zone, the reactant solution is cooled by a jacket cooler and released from a back-pressure regulator. This setup for hydrothermal synthesis enables the rapid heating of a reactant solution, which leads to the production of smaller nanoparticles, and many studies have been performed using flow-type hydrothermal reactors.

However, studies using flow-type reactors also revealed that the mixing configuration affected the size and size distribution of the produced nanoparticles. We further determined that the orientation of the heated water and reactant solution streams with respect to the direction of gravity affected the size of the produced nanoparticles.[16] This behavior suggested that the reaction rate of metal ions was fast and that the products were affected by the course of mixing. Therefore, it is important to determine the course of mixing in the mixers of flow-type hydrothermal reactors. However, the course of mixing is difficult to visualize because flow-type reactors that maintain a high pressure at elevated temperatures are composed of stainless steel. Several studies were performed that involved obtaining X-ray diffraction patterns of metal oxide nanoparticles that were produced inside flow-type reactors.[17–19] Even so, direct observation of the mixing behavior of water streams is still difficult. A possible method for evaluating the course of mixing in mixers is numerical simulation. However, the curve for the heat capacity of water around the critical point has a cusp, and numerical simulation across the critical temperature is rather difficult. Based on this background, we used neutron radiography measurements to study the course of mixing in a supercritical flow-type reactor.[16,20–22]

Neutron radiography is a method for determining the internal structure of objects with transmitted neutron beams.[23,24] While hydrogen atoms effectively attenuate the neutron beam, metal elements, including iron, chromium, and nickel, are almost transparent. In flow-type hydrothermal reactors, the back-pressure regulator controls the pressure inside the reactor at approximately 25 MPa. Therefore, supercritical water has a lower density, ~0.2 g cm^{-3}, while the density of room-temperature water is approximately 1.0 g cm^{-3} inside the reactor. We expected that the neutron beam shows the difference in the density of water, which corresponds to the temperature, in stainless steel mixers. Based on this concept, we performed neutron radiography measurements on an operating flow-type reactor using distilled water instead of a metal ion solution. The obtained radiographic images clearly showed the mixing behavior of supercritical water (lower water density) and room-temperature water (higher water density) in a T-shaped mixer, as shown in Fig. 2b.[21] The images showed that supercritical water supplied from the top penetrated the side tube where room-temperature water was supplied. The images also showed that room-temperature water followed a downward path along the wall of the vertical tube after passing the mixing point. These images indicated that with the T-shaped mixer used in the previous study, it was difficult to instantaneously mix the supercritical water and room-temperature water at the mixing point.

To date, several research groups have designed and compared mixer shapes for mixing heated water and room-temperature water more rapidly in flow-type hydrothermal synthesis.[25–36] Lester *et al.* developed a countercurrent reactor to overcome the shortcomings of the conventional T-shaped mixer and synthesized metal oxide nanoparticles.[25,26] Kawasaki *et al.* proposed a swirl mixer to efficiently mix supercritical water and the reactant solution.[27,28] Darr *et al.* designed a confined jet mixer and synthesized metal oxide nanoparticles under various conditions.[29,30] Yan *et al.* used a small orifice for the heated water stream in the center of the T-shaped mixer.[31] The effects of narrowed inlet channels were also studied by Li *et al.* in terms of process intensification.[37] In our study, we proposed a mixer for the instantaneous heating of the reactant solution and performed neutron radiography measurements to confirm how supercritical water and room-temperature water mixed in the proposed mixer. We also conducted supercritical hydrothermal CeO_2 nanoparticle synthesis using the conventional and proposed mixers while varying the flow rates of the aqueous solution and supercritical water. The proposed new mixer shape and method for observing the mixing behavior using a neutron beam in the actual apparatus for hydrothermal synthesis are expected to provide vital insight for improving metal oxide nanoparticle synthesis using flow-type reactors.

Experimental

Neutron radiography of the mixing process of supercritical water and room-temperature water

In this study, we conducted neutron radiography measurements to visualize the mixing behavior in the proposed mixer in a flow-type reactor. The measurements were performed at the B4 port of the Kyoto University Reactor (KUR) at the Institute for Integrated Radiation and Nuclear

Science, Kyoto University. The KUR was operated at a 5 MW output with a neutron flux of *ca.* 5×10^7 n cm^{-2} s at the beam exit of the B4 neutron guide tube. The experimental setup was similar to that used in previous studies,[20–22] and the tubes and components that the heated water stream passed through were covered by a thermal insulator. As shown in Fig. 3, the mixer in the flow-type reactor was placed along the thermal neutron beam path from the nuclear reactor.

The neutron beam that passed through the mixer was converted into fluorescent light using a 200 μm-thick ^{6}LiF/ZnS scintillator screen; a charge-coupled device camera (BITRAN BU-53LN) with a 180 mm telephoto lens (SIGMA APO MACRO DG HSM, f = 3.5) was used to capture the fluorescent light. The imaging area, resolution, and bit depth were 42 × 42 mm^2, 1024 × 1024, and 16 bits, respectively. The exposure time for one image was 30 s, and 10 images were acquired for each mixing condition. The acquired images were processed as described later in this paper.

In this study, we developed a new mixer shape for the flow-type hydrothermal reactor, as shown in Fig. 4. The mixer was assembled by simply inserting a 1/16 inch tube with an inner diameter of 1.0 mm into a Swagelok 1/8 inch T-shaped junction (inner diameter: 2.3 mm) from the side. By inserting the narrower tube into the T-shaped component, we expected the reactant solution to flow from the center of the vertical tube. The narrower tube was also expected to prevent the penetration of supercritical water in the side tube. We operated the flow-type hydrothermal reactor and performed neutron radiography with both the conventional and proposed mixer. In this study, pure water at room-temperature was supplied instead of an aqueous metal ion solution because the metal ion concentration was low during synthesis and its effect on mixing was negligible. The operating conditions are summarized in Table 1. Supercritical water was supplied from the top, while room-temperature water was supplied from the side. The back-pressure regulator controlled the pressure inside the reactor at 25 MPa.

The neutron radiography images acquired under the above experimental conditions were processed as follows to obtain images of the average water density in the mixer. After obtaining the neutron radiography images for all mixing

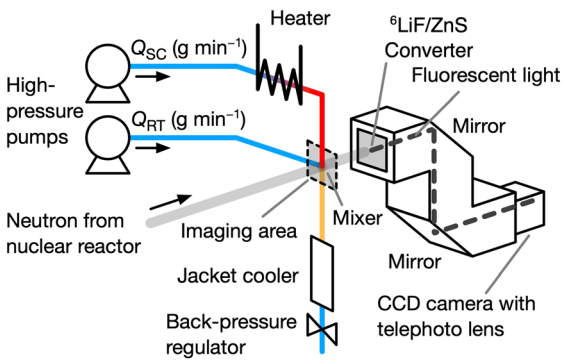

Fig. 3 Diagram of the experimental apparatus.

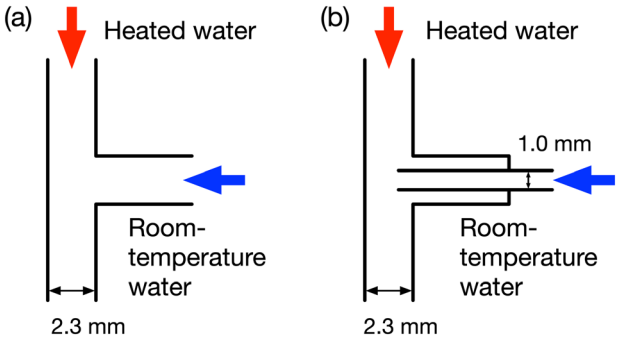

Fig. 4 Schematic of the (a) conventional and (b) proposed mixer.

conditions (I, Fig. 5a), the heater of the flow-type reactor was turned off while water streams were supplied to cool the mixer. A neutron radiography image was acquired when the mixer was filled with room-temperature water (I_{fill}, Fig. 5b). Then, air flow was fed into the mixer to completely replace the water with air. After confirming that the mixture was completely dried, a neutron radiography image was acquired (I_{empty}, Fig. 5c). The flow-type reactor was then removed from the neutron beam path, and a two-dimensional distribution profile of the incident neutron beam was obtained (I_{flat}, Fig. 5d). Finally, we measured the dark noise of the camera by acquiring an image without neutron irradiation (I_{dark}, Fig. 5e). For each of these images, the exposure time was 30 s, and 10 images were acquired for each condition.

The obtained radiographic images were analyzed using ImageJ[38] software as follows. First, the hot pixels were removed using the 'Despeckle' function, and the 10 images acquired under the same conditions were averaged. Then, the absorbance (A) under each mixing condition was calculated using eqn (1) considering the effect of the dark noise and the profile of the irradiated neutron beam.

$$A = -\ln \frac{I - I_{dark}}{I_{flat} - I_{dark}} \quad (1)$$

The images of the mixer filled with room-temperature water and air were similarly processed. The acquired images are shown in Fig. 6. Since the acquired images were the superimposition of the mixer and the water in the mixer, an average water density profile (D) of the mixer was obtained as follows:

Table 1 Flow rates of supercritical water (Q_{SC}) and room-temperature water (Q_{RT})

Q_{SC} (g min^{-1})	Q_{RT} (g min^{-1})		
8.0	2.0	4.0	8.0
12.0	3.0	6.0	12.0
16.0	4.0	8.0	16.0
20.0	5.0	10.0	15.0[a]

[a] Q_{RT} was set to 15.0 g min^{-1} at Q_{SC} = 20.0 g min^{-1} due to the capacity of the jacket cooler.

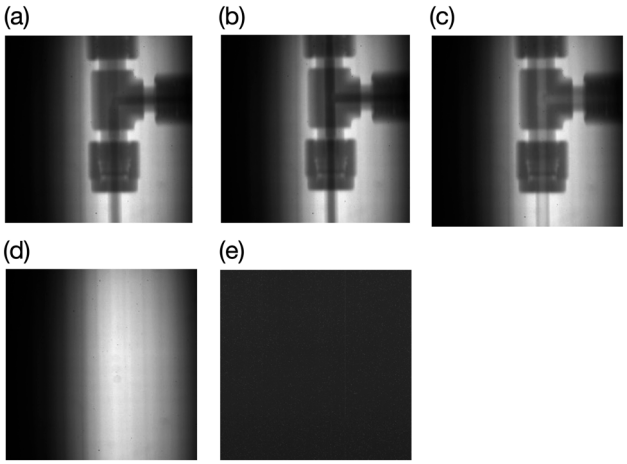

Fig. 5 Neutron radiographic images of the (a) mixer during operation (I), (b) mixer filled with room-temperature water (I_{fill}), (c) mixer filled with air (I_{empty}), (d) incident neutron beam (I_{flat}), and (e) dark noise of the camera (I_{dark}).

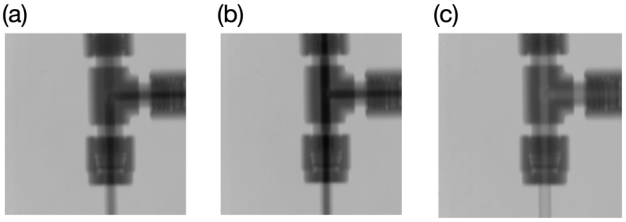

Fig. 6 Neutron absorbance profile of the mixer (a) under operating conditions (A), (b) filled with room-temperature water (A_{fill}), and (c) filled with air (A_{empty}).

$$D = \frac{A - A_{empty}}{A_{fill} - A_{empty}} \quad (2)$$

Because of the thermal expansion of the mixer and other components, the calculated absorbance images were scaled and rotated to fit with each other. The calculated images that appear later in this paper show the average water density along the neutron beam direction inside the mixer. The images were also calculated as time-averaged results over the 30 s exposure time.

CeO_2 nanoparticle synthesis using a flow-type supercritical hydrothermal reactor

In this study, CeO_2 nanoparticles were synthesized to determine how the mixer shape affects the size of the produced nanoparticles under various mixing conditions. CeO_2 nanoparticles were synthesized using the same flow-type reactor used in the neutron radiography measurements. An aqueous solution of $Ce(NO_3)_3$ with a concentration of 0.010 mol L^{-1} was used as the reactant. The streams of heated water and the reactant solution were mixed in the same mixer under various mixing conditions. The mixed stream was cooled by a jacket cooler and released from a back-pressure regulator. The pressure in the reactor was maintained at 25 MPa using the back-pressure regulator. The product suspension was centrifuged to purify the solid products. The crystal structure of the products was confirmed by X-ray diffraction (XRD, Panalytical Aeris), and the size of the nanoparticles was evaluated using scanning electron microscopy (SEM, JEOL JSM-7500A). The average size and size distribution of the produced nanoparticles were evaluated by measuring the Ferret diameter using 100 samples for one synthesis condition.

Results and discussion

First, we discuss the effects of the mixer shape on the mixing behavior. Fig. 7 shows the average water density profiles of both mixers when the flow rates of the supercritical water (Q_{SC}) and room-temperature water (Q_{RT}) were Q_{SC} = 8.0 and Q_{RT} = 2.0 g min^{-1}, and Q_{SC} = 12.0 and Q_{RT} = 3.0 g min^{-1}. The temperatures of the streams are shown in Fig. 7.

In Fig. 7, the darker area corresponds to a higher water density, which corresponds to a lower temperature. Fig. 7a and b show that room-temperature water supplied from the side flowed along the right wall of the vertical tube after mixing under both mixing conditions in the conventional mixer. The supercritical water supplied from the top flowed along the left side of the vertical tube, and the two streams gradually mixed. Moreover, the penetration of supercritical water into the upper part of the side tube was clearly observed, as indicated in Fig. 7a, when the flow rate of room-temperature water was lower than that shown in Fig. 7b. The tendencies of mixing were apparently different for the proposed mixer shown in Fig. 7c and d. The end of the inserted tube was positioned slightly above the midpoint, possibly because of thermal expansion of the components. The stream of room-temperature water flowed out from the side tube with an inner diameter of 1.0 mm and uniformly mixed with the supercritical water supplied from the top. The supercritical water did not penetrate into the side tube, possibly due to the narrower inner diameter of 1.0 mm. In

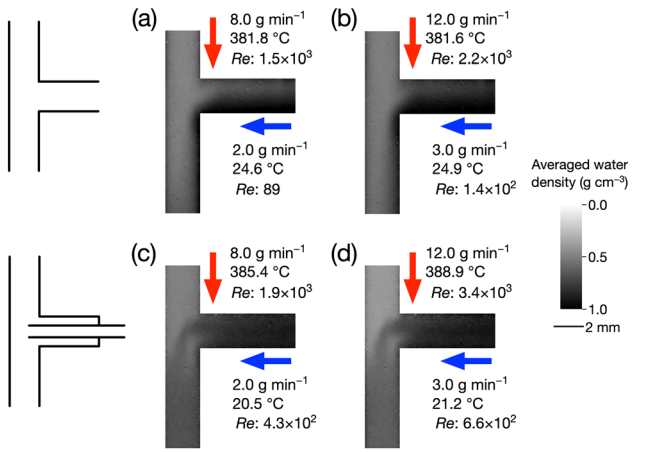

Fig. 7 Average water density profiles of the (a and b) conventional and (c and d) proposed mixers.

our previous study, using the conventional mixer shown in Fig. 7a and b, we determined that the reactant solution supplied from the side was gradually heated in the side and vertical tubes. This mixing behavior resulted in a lower heating rate of the reactant solution, which caused gradual hydrothermal reactions and nanoparticle nucleation. In other words, this mixing behavior possibly promoted the synthesis of larger nanoparticles with a broader size distribution. Conversely, the mixer proposed in this study solved these problems, as shown in Fig. 7c and d. The supplied room-temperature water quickly mixed in the vertical tube after the T-junction. Therefore, the proposed mixer was expected to produce metal oxide nanoparticles with smaller sizes and a narrower size distribution.

We then evaluated the effects of the flow rates of supercritical water and room-temperature water on the mixing behavior using the proposed mixer. Fig. 8–10 show the average water density in the proposed mixer under various mixing conditions. When the ratio of $Q_{SC}:Q_{RT}$ was 4 : 1 (Fig. 8), a stream of room-temperature water flowed out from the side tube (smaller diameter) inserted into the center of the vertical tube (larger diameter). Then, the stream flowed downward with the flow of supercritical water, and the boundary between the two streams quickly disappeared. This tendency was observed under all mixing conditions with a $Q_{SC}:Q_{RT}$ of 4 : 1. When $Q_{SC}:Q_{RT}$ was 2 : 1 (Fig. 9), similar average water density profiles were obtained, but a portion of the room-temperature stream approached the left sidewall of the vertical tube. This tendency was clearly confirmed when $Q_{SC}:Q_{RT}$ was 1 : 1 (Fig. 10). Under these mixing conditions, the streams of room-temperature water collided with the left side of the inner wall of the vertical tube. The streams then mixed with the supercritical water supplied from the top. These trends indicated that the ratio of the flow rates, $Q_{SC}:Q_{RT}$, was the main determinant of the mixing behavior in the proposed mixer. When $Q_{SC}:Q_{RT}$ was 4 : 1 (Fig. 8), the streams of room-temperature water were released at the center of the vertical tube and mixed with the supercritical water. Conversely, the streams of room-temperature water collided with the left wall of the vertical tube and mixed with the supercritical water when $Q_{SC}:Q_{RT}$ was 1 : 1 (Fig. 10).

We then compared the average water density profiles under various mixing conditions. Fig. 11 shows the average water density at the center of the vertical tube along the flow direction. Fig. 12 shows the average water density along the diameter of the vertical tube just after the junction. Fig. 11a and b and 12a and b show the average water density in the conventional mixer, whereas Fig. 11c and d and 12c and d show the average water density in the proposed mixer. In Fig. 11, the dotted lines correspond to the top and bottom of the side tube where the stream of the room-temperature water flowed out. As shown in Fig. 11a and b, the average water density gradually increased after mixing in the conventional mixer, as previously shown in Fig. 7a and b. Conversely, the average water density rapidly increased after mixing in the proposed mixer, as shown in Fig. 11c and d. By comparing the

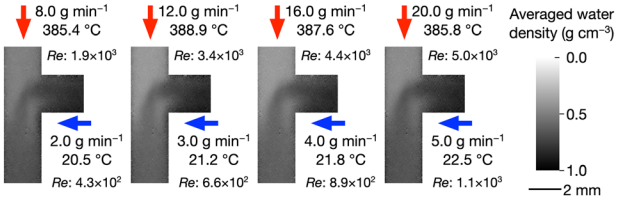

Fig. 8 Average water density profile under the proposed mixing conditions when $Q_{SC}:Q_{RT}$ was 4 : 1.

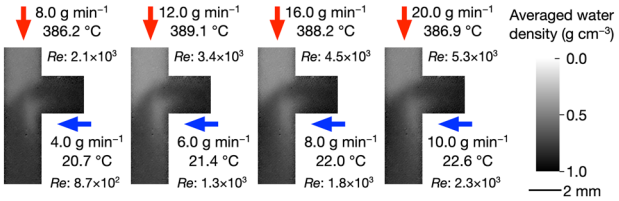

Fig. 9 Average water density profile under the proposed mixing conditions when $Q_{SC}:Q_{RT}$ was 2 : 1.

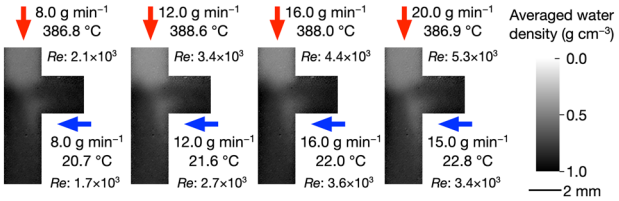

Fig. 10 Average water density profile under the proposed mixing conditions when $Q_{SC}:Q_{RT}$ was 1 : 1.

results shown in Fig. 11, we confirmed that the proposed mixer quickly mixes supercritical water and room-temperature water. Moreover, the water density rapidly increased as the flow rate of the room-temperature water increased. Fig. 12 shows the average water density along the diameter at the bottom of the junction. In our measurements, the stream of room-temperature water flowed from the right. Therefore, the water density on the right side of the vertical tube was larger than that on the left side in the conventional mixer (Fig. 12a and b). However, the water density was more uniform in the proposed mixer (Fig. 12c and d). When $Q_{SC}:Q_{RT}$ was 4 : 1, the water density at the center of the vertical tube was slightly higher than that in the region close to the wall because room-temperature water flowed out around the center of the vertical tube and quickly mixed with supercritical water. When $Q_{SC}:Q_{RT}$ was 1 : 1, the average water density on the left side of the vertical tube was larger than that on the right side because room-temperature water with a high flow rate exited with a high flow velocity and collided with the wall on the left side of the vertical tube.

The neutron radiography results showed that compared to the conventional mixer, the proposed mixer provided rapid mixing of supercritical water with room-temperature water;

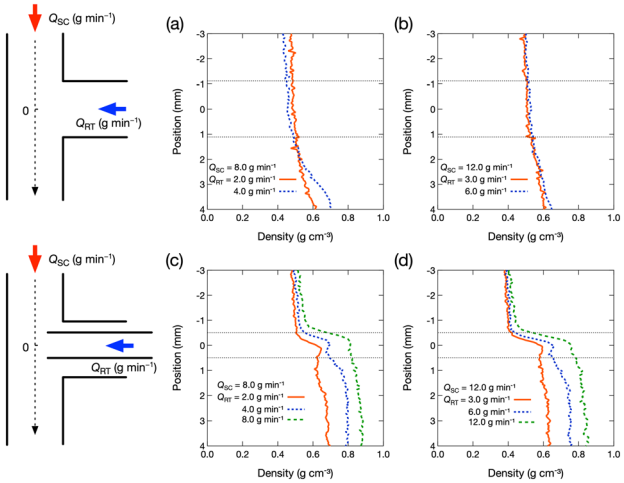

Fig. 11 Distribution of the average water density at the center of the vertical tube in (a) and (b) the conventional mixer and (c) and (d) the proposed mixer. The flow rate of the supercritical water (Q_{SC}) was (a) and (c) 8.0 g min^{-1} and (b) and (d) 12.0 g min^{-1}. The flow rate of the room-temperature water (Q_{RT}) is shown in the figure.

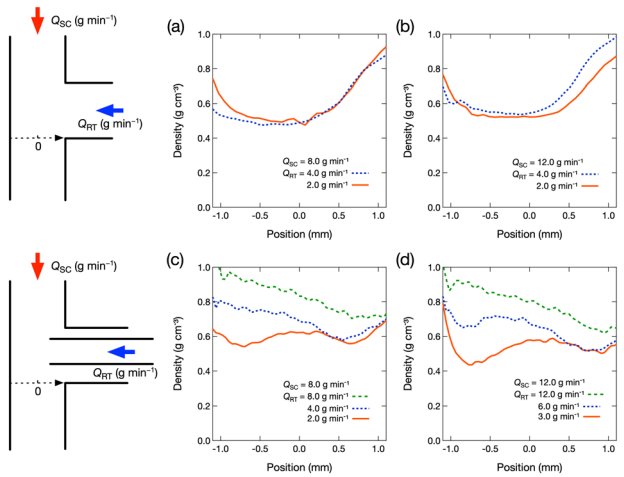

Fig. 12 Distribution of the average water density along the diameter in (a) and (b) the conventional mixer and (c) and (d) the proposed mixer. The flow rate of the supercritical water (Q_{SC}) was (a) and (c) 8.0 g min^{-1} and (b) and (d) 12.0 g min^{-1}. The flow rate of the room-temperature water (Q_{RT}) is shown in the figure.

these results suggested that the proposed mixer produced smaller metal oxide nanoparticles with a narrower size distribution. To confirm the effects of the mixer, we then synthesized CeO_2 nanoparticles using the conventional and proposed mixers. Fig. 13 and 14 show the SEM images and the size distribution of the CeO_2 nanoparticles produced using the conventional and proposed mixers under flow conditions when $Q_{SC}:Q_{RT}$ was 4 : 1. The produced CeO_2 nanoparticles had an octahedral shape surrounded by thermodynamically stable {111} crystal planes.

The average sizes were smaller and the size distributions were narrower under both flow rate conditions when we used the proposed mixer (Fig. 13 and 14), possibly because the

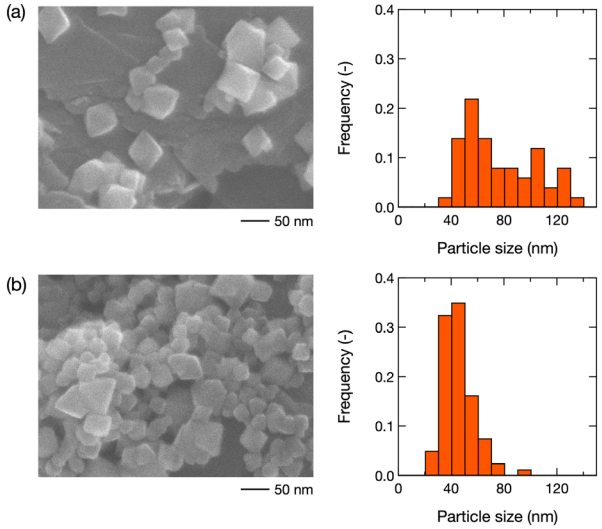

Fig. 13 SEM image and size distribution of CeO_2 nanoparticles produced using the (a) conventional and (b) proposed mixer when Q_{SC} = 8.0 and Q_{RT} = 2.0 g min^{-1}.

supercritical water and reactant solution were more rapidly mixed, as confirmed using neutron radiography. The rapid mixing possibly promoted a faster reaction of metal ions and resulted in a higher degree of supersaturation and the synthesis of smaller nanoparticles. The rapid mixing also inhibited the growth of the produced nanoparticles. Therefore, the average size and size distribution of the nanoparticles decreased. We also evaluated the size of the produced CeO_2 nanoparticles when $Q_{SC}:Q_{RT}$ was 1 : 1 and 2 : 1. The results are summarized in Fig. 15.

The average size was smaller and the size distribution was narrower with the proposed mixer for all mixing conditions. Therefore, the proposed mixer was confirmed to be more suitable for synthesizing smaller metal oxide nanoparticles.

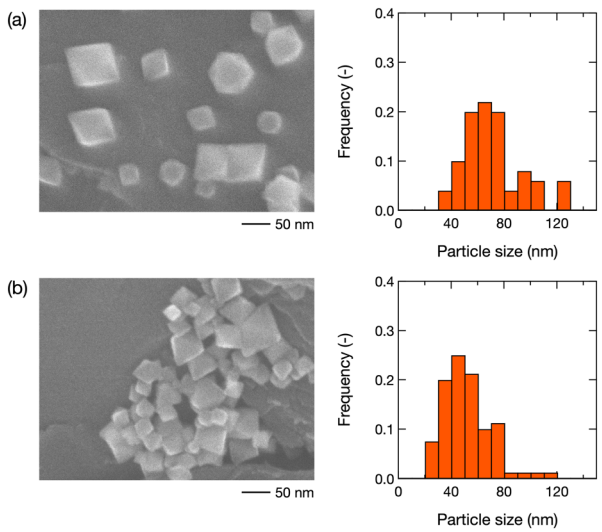

Fig. 14 SEM image and size distribution of CeO_2 nanoparticles produced using the (a) conventional and (b) proposed mixer when Q_{SC} = 12.0 and Q_{RT} = 3.0 g min^{-1}.

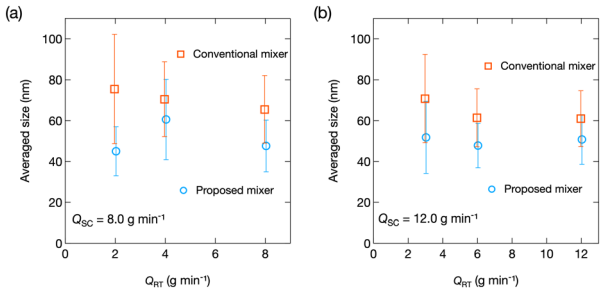

Fig. 15 Average size and standard deviation of CeO_2 nanoparticles synthesized using the conventional and proposed mixer when Q_{SC} was (a) 8.0 g min^{-1} and (b) 12.0 g min^{-1}.

The use of a narrower tube inserted into the conventional mixer might also have reduced the chance that the reactant solution was heated before mixing. The mixer component of the conventional mixer was heated by thermal conduction from the top where the supercritical water was supplied. As a result, the reactant solution, which contacted the mixer component, was heated before mixing in the mixer component. Conversely, the inserted narrower tube in the proposed mixer was fixed at the edge of the mixer component, and thermal conduction was limited. Therefore, the reactant solution was heated less in the proposed mixer before mixing, which possibly resulted in instantaneous heating by mixing. This behavior might also have contributed to the higher degree of supersaturation and the production of smaller nanoparticles.

Conclusions

In this study, we compared the mixing behavior of supercritical water and room-temperature water using conventional and proposed mixers in a flow-type hydrothermal reactor by neutron radiography. We further performed supercritical hydrothermal CeO_2 nanoparticle synthesis using the conventional and proposed mixers. We determined that the proposed mixer provided more rapid mixing than the conventional mixer under various flow conditions. The penetration of supercritical water into the side tube and the partitioned flow behavior in the vertical tube after mixing were prevented in the proposed mixer. These behaviors resulted in the rapid mixing of the streams, as shown in the temperature profile of the center of the vertical tube. In addition, the proposed mixer reduced the heating of the metal ion solution in the side tube. We then synthesized CeO_2 nanoparticles using the conventional and proposed mixers. The proposed mixer produced CeO_2 nanoparticles with a smaller size and narrower distribution because of the rapid mixing of the reactant solution with the supercritical water. Neutron radiography measurements could be useful for visualizing various processes involving supercritical water that use equipment with thick metal walls to maintain a high pressure at elevated temperatures. We also believe that neutron radiography measurements could be applicable for visualizing the mixing behavior of streams with different hydrogen densities, for instance, different organic solvents or an organic solvent at different temperatures.

Author contributions

Kosei Sato: formal analysis, investigation, visualization, writing – original draft. Ryosuke Sasaki: investigation. Bo Xie: investigation. Seiichi Takami: conceptualization, funding acquisition, project administration, resources, writing – review & editing. Masaki Kubo: conceptualization, investigation. Takao Tsukada: conceptualization. Katsumi Sugimoto: methodology. Naoya Odaira: methodology, resources. Daisuke Ito: methodology, resources. Yasushi Saito: methodology, resources. All authors have given their approval of the final version of the manuscript.

Conflicts of interest

There are no conflicts to declare.

Acknowledgements

This research was supported in part by JSPS KAKENHI Grant Numbers 17H06467 and 20H02514. Neutron radiography measurements were performed under the Visiting Researchers Program of the Institute for Integrated Radiation and Nuclear Science, Kyoto University.

Notes and references

1 H. You, S. Yang, B. Ding and H. Yang, *Chem. Soc. Rev.*, 2012, **42**, 2880–2904.
2 M. Azharuddin, G. H. Zhu, D. Das, E. Ozgur, L. Uzun, A. P. F. Turner and H. K. Patra, *Chem. Commun.*, 2019, **55**, 6964–6996.
3 Y. Shi, Z. Lyu, M. Zhao, R. Chen, Q. N. Nguyen and Y. Xia, *Chem. Rev.*, 2021, **121**, 649–735.
4 J. A. Darr, J. Zhang, N. M. Makwana and X. Weng, *Chem. Rev.*, 2017, **117**, 11125–11238.
5 M. Parashar, V. K. Shukla and R. Singh, *J. Mater. Sci.: Mater. Electron.*, 2020, **31**, 3729–3749.
6 M. S. Whittingham, *Curr. Opin. Solid State Mater. Sci.*, 1996, **1**, 227–232.
7 S. Feng and R. Xu, *Acc. Chem. Res.*, 2001, **34**, 239–247.
8 Y. Hakuta, H. Hayashi and K. Arai, *Curr. Opin. Solid State Mater. Sci.*, 2003, **7**, 341–351.
9 C. Aymonier, A. Loppinet-Serani, H. Reverón, Y. Garrabos and F. Cansell, *J. Supercrit. Fluids*, 2006, **38**, 242–251.
10 K. Byrappa and T. Adschiri, *Prog. Cryst. Growth Charact.*, 2007, **53**, 117–166.
11 H. Hayashi and Y. Hakuta, *Materials*, 2010, **3**, 3794–3817.
12 T. Adschiri, Y.-W. Lee, M. Goto and S. Takami, *Green Chem.*, 2011, **13**, 1380–1390.
13 D. P. Fernández, A. R. H. Goodwin, E. W. Lemmon, J. M. H. L. Sengers and R. C. Williams, *J. Phys. Chem. Ref. Data*, 1997, **26**, 1125–1166.

14 T. Adschiri, K. Kanazawa and K. Arai, *J. Am. Ceram. Soc.*, 1992, **75**, 2615–2618.
15 Y. Xu, V. Musumeci and C. Aymonier, *React. Chem. Eng.*, 2019, **4**, 2030–2054.
16 K. Sugioka, K. Ozawa, M. Kubo, T. Tsukada, S. Takami, T. Adschiri, K. Sugimoto, N. Takenaka and Y. Saito, *J. Supercrit. Fluids*, 2016, **109**, 43–50.
17 V. Middelkoop, P. Boldrin, M. Peel, T. Buslaps, P. Barnes, J. A. Darr and S. D. M. Jacques, *Chem. Mater.*, 2009, **21**, 2430–2435.
18 V. Middelkoop, C. J. Tighe, S. Kellici, R. I. Gruar, J. M. Perkins, S. D. M. Jacques, P. Barnes and J. A. Darr, *J. Supercrit. Fluids*, 2014, **87**, 118–128.
19 A. Yoko, M. Akizuki, N. Hirao, S. Kohara, M. Kumar, N. Umezawa, T. Ohno and Y. Oshima, *J. Supercrit. Fluids*, 2016, **107**, 746–752.
20 S. Takami, K. Sugioka, T. Tsukada, T. Adschiri, K. Sugimoto, N. Takenaka and Y. Saito, *J. Supercrit. Fluids*, 2012, **63**, 46–51.
21 K. Sugioka, K. Ozawa, T. Tsukada, S. Takami, T. Adschiri, K. Sugimoto, N. Takenaka and Y. Saito, *AIChE J.*, 2014, **60**, 1168–1175.
22 S. Takami, K. Sugioka, K. Ozawa, T. Tsukada, T. Adschiri, K. Sugimoto, N. Takenaka and Y. Saito, *Phys. Procedia*, 2015, **69**, 564–569.
23 M. Strobl, I. Manke, N. Kardjilov, A. Hilger, M. Dawson and J. Banhart, *J. Phys. D: Appl. Phys.*, 2009, **42**, 243001.
24 K. M. Podurets, S. E. Kichanov, V. P. Glazkov, E. S. Kovalenko, M. M. Murashev, D. P. Kozlenko, E. V. Lukin and E. B. Yatsishina, *Crystallogr. Rep.*, 2021, **66**, 254–266.
25 E. Lester, P. Blood, J. Denyer, D. Giddings, B. Azzopardi and M. Poliakoff, *J. Supercrit. Fluids*, 2006, **37**, 209–214.
26 P. W. Dunne, A. S. Munn, C. L. Starkey, T. A. Huddle and E. H. Lester, *Philos. Trans. R. Soc., A*, 2015, **373**, 20150015.
27 Y. Wakashima, A. Suzuki, S. Kawasaki, K. Matsui and Y. Hakuta, *J. Chem. Eng. Jpn.*, 2007, **40**, 622–629.
28 S. Kawasaki, K. Sue, R. Ookawara, Y. Wakashima and A. Suzuki, *J. Oleo Sci.*, 2010, **59**, 557–562.
29 R. I. Gruar, C. J. Tighe and J. A. Darr, *Ind. Eng. Chem. Res.*, 2013, **52**, 5270–5281.
30 C. J. Denis, C. J. Tighe, R. I. Gruar, N. M. Makwana and J. A. Darr, *Cryst. Growth Des.*, 2015, **15**, 4256–4265.
31 X. Yan, W. Trevillyan, I. Castano, Y. Sun, R. Muehleisen and J. Li, *J. Nanomater.*, 2019, **2019**, 2570698.
32 L. L. Toft, D. F. Aarup, M. Bremholm, P. Hald and B. B. Iversen, *J. Solid State Chem.*, 2009, **182**, 491–495.
33 A. Aimable, H. Muhr, C. Gentric, F. Bernard, F. L. Cras and D. Aymes, *Powder Technol.*, 2009, **190**, 99–106.
34 F. Demoisson, M. Ariane, A. Leybros, H. Muhr and F. Bernard, *J. Supercrit. Fluids*, 2011, **58**, 371–377.
35 P. Zielke, Y. Xu, S. B. Simonsen, P. Norby and R. Kiebach, *J. Supercrit. Fluids*, 2016, **117**, 1–12.
36 J. Hiemer, A. Clausing, T. Schwarz and K. Stwöwe, *Chem. Eng. Technol.*, 2019, **42**, 2018–2027.
37 G. Li, X. Pu, M. Shang, L. Zha and Y. Su, *AIChE J.*, 2019, **65**, 334–346.
38 W. S. Rasband, ImageJ, 1997–2018, U. S. National Institutes of Health, Bethesda, Maryland, USA, **https://imagej.nih.gov/ij/**.